

# Controlling the quantum stereodynamics of ultracold bimolecular reactions

M. H. G. de Miranda,<sup>1\*</sup> A. Chotia,<sup>1\*</sup> B. Neyenhuis,<sup>1\*</sup> D. Wang,<sup>1\*§</sup>

G. Quéméner,<sup>1</sup> S. Ospelkaus,<sup>1</sup> J. L. Bohn,<sup>1</sup> J. Ye,<sup>1†</sup> D. S. Jin<sup>1†</sup>

<sup>1</sup>*JILA, NIST and University of Colorado,*

*Department of Physics University of Colorado*

*Boulder, CO 80309-0440, USA*

*\*These authors contributed equally to this work;*

*§Present address: Department of Physics,*

*The Chinese University of Hong Kong;*

*†To whom correspondence should be addressed;*

*E-mail: Ye@jila.colorado.edu; Jin@jilau1.colorado.edu*

PACS numbers: XXX

arXiv:1010.3731v1 [quant-ph] 18 Oct 2010

Chemical reaction rates often depend strongly on stereodynamics, namely the orientation and movement of molecules in three-dimensional space [1–3]. An ultracold molecular gas, with a temperature below 1  $\mu\text{K}$ , provides a highly unusual regime for chemistry, where polar molecules can easily be oriented using an external electric field and where, moreover, the motion of two colliding molecules is strictly quantized. Recently, atom-exchange reactions were observed in a trapped ultracold gas of KRb molecules [4]. In an external electric field, these exothermic and barrierless bimolecular reactions,  $\text{KRb} + \text{KRb} \rightarrow \text{K}_2 + \text{Rb}_2$ , occur at a rate that rises steeply with increasing dipole moment [5]. Here we show that the quantum stereodynamics of the ultracold collisions can be exploited to suppress the bimolecular chemical reaction rate by nearly two orders of magnitude. We use an optical lattice trap to confine the fermionic polar molecules in a quasi-two-dimensional, pancake-like geometry, with the dipoles oriented along the tight confinement direction [6, 7]. With the combination of sufficiently tight confinement and Fermi statistics of the molecules, two polar molecules can approach each other only in a “side-by-side” collision, where the chemical reaction rate is suppressed by the repulsive dipole-dipole interaction. We show that the suppression of the bimolecular reaction rate requires quantum-state control of both the internal and external degrees of freedom of the molecules. The suppression of chemical reactions for polar molecules in a quasi-two-dimensional trap opens the way for investigation of a dipolar molecular quantum gas. Because of the strong, long-range character of the dipole-dipole interactions, such a gas brings fundamentally new abilities to quantum-gas-based studies of strongly correlated many-body physics, where quantum phase transitions and new states

**of matter can emerge [8–13].**

Two colliding polar molecules interact via long-range dipole-dipole forces well before they reach the shorter distance scales where chemical forces become relevant. Therefore, the spatial anisotropy of the dipolar interaction can play an essential role in the stereochemistry of bimolecular reactions of polar molecules. In general, one expects the attraction between oriented dipoles in a “head-to-tail” collision to be favorable for chemical reactions, while the repulsion between two oriented polar molecules in a “side-by-side” collision presents an obstacle for reactions. Up to now, however, large center-of-mass collision energies have precluded the direct control of chemical reactions via dipolar interactions. In a cold collision regime, where tens of scattering partial waves contribute, one can begin to exert control of intermolecular dynamics through the dipolar effect [14]. An ultracold gas, however, provides an optimum environment in which to fully investigate the dipolar effects [5, 15, 16]. Here, the molecules can be prepared in identical internal quantum states, with the dipoles oriented using an external electric field, and the molecular gas confined in external potentials created using light. In the limit of vanishing collision energies, the stereodynamics is described by only a few quantized collision channels, and, moreover, for indistinguishable molecules, the states of translational motion are coupled to internal molecular states due to the fact that the quantum statistics of the molecules (fermions or bosons) dictates a particular symmetry of the total wavefunction with respect to exchange of two molecules. In this quantum regime, we have an opportunity to suppress or enhance reaction rates by understanding and precisely controlling the stereodynamics of colliding polar molecules.

The spatial geometry of the confining potential can influence collisions in a trapped gas of polar molecules. In particular, a two-dimensional (2D) trap geometry, with the dipoles oriented parallel to the tight confinement direction  $\hat{z}$ , is well-matched to the spatial

anisotropy of the dipole-dipole interaction [17–19]. We can realize such a geometry using a one-dimensional optical lattice (see Fig. 1 A), where the trapped molecules are divided among several isolated layers. In each of these layers, the lattice potential provides tight harmonic confinement in  $\hat{z}$  such that only the lowest few quantized motional states in  $\hat{z}$  are occupied. Consequently, within each isolated layer, colliding molecules approach each other in 2D. However, the range of the van der Waals interaction (and, for that matter, the range of dipolar interactions at our largest external electric field) is still smaller than the spatial extent of the cloud in the direction of tight confinement,  $a_{ho}$ , and, therefore, at short intermolecular distances a collision still must be treated in three dimensions (3D).

We now consider the quantized collision channels that define the stereodynamics in this quasi-2D geometry. For intermolecular separations that are much larger than  $a_{ho}$ , the relative motion of the two molecules is described by a quantized angular momentum,  $\hbar M$ , around the  $\hat{z}$  axis, where  $\hbar = \frac{h}{2\pi}$  and  $h$  is Planck’s constant, as well as by a quantized relative motion along  $\hat{z}$ . As discussed above, the stereodynamics of ultracold collisions of indistinguishable molecules is strongly influenced by the fact that the two-molecule wavefunction must obey an overall symmetry with respect to the exchange of the identical molecules. Therefore, an essential aspect of relative motion in  $\hat{z}$  is the exchange symmetry of this part of the two-molecule wavefunction, which we identify with a quantum number  $\gamma$ ; for the symmetric case,  $\gamma = 1$  and for the antisymmetric case,  $\gamma = -1$ . For two molecules in the same  $\hat{z}$  harmonic oscillator state,  $\gamma = 1$ ; while both  $\gamma = 1$  and  $\gamma = -1$  are possible for two molecules in different harmonic oscillator states. Similarly, we use a quantum number  $\eta$  to keep track of the exchange symmetry of the part of the wavefunction that describes the internal states of the two molecules. For two molecules in the same internal quantum state,  $\eta = 1$ , while  $\eta = \pm 1$  for molecules in different internal states. In 2D, these three quantum

numbers  $(M, \gamma, \eta)$  are sufficient to describe the quantum stereodynamics. However, because the interactions at short range must be described in 3D, the quantum number corresponding to the 3D angular momentum,  $L$ , as well as  $M$ , becomes relevant. With collisional channels described by quantum numbers  $\eta, L, \gamma$ , and  $M$ , the fermionic symmetry can be concisely stated in the following relations:

$$\eta(-1)^L = -1, \quad \text{Short range, 3D} \quad (1)$$

$$\eta\gamma(-1)^M = -1. \quad \text{Long range, 2D} \quad (2)$$

For ultracold collisions, the chemical reaction rate will be dominated by the allowed collision channel with the lowest centrifugal barrier. Combining this fact with the relations above, we identify three collision channels relevant to the stereodynamics, and we label these  $|1\rangle$ ,  $|2\rangle$ , and  $|3\rangle$ , in order of increasing centrifugal barrier heights. The dipole-dipole interaction mixes states with different  $L$ . However, for convenience, we will refer to the lowest energy adiabatic channel, which does not have a centrifugal barrier, as  $L = 0$ . Similarly, we will use  $L = 1$  to denote the odd- $L$  adiabatic channel with the lowest centrifugal barrier. Collision channel  $|1\rangle$  has  $\eta = -1$ ,  $L = 0$ ,  $\gamma = 1$ , and  $M = 0$ , and corresponds to spatially isotropic collisions. Collision channel  $|2\rangle$  has  $\eta = 1$ ,  $L = 1$ ,  $\gamma = -1$ , and  $M = 0$ , and is the quantum analog of “head-to-tail” collisions. Collision channel  $|3\rangle$  has  $\eta = 1$ ,  $L = 1$ ,  $\gamma = 1$ , and  $M = \pm 1$ , and is the quantum analog of “side-by-side” collisions. Fig. 1 B shows schematically the adiabatic potentials for these three lowest energy collision channels. Channels  $|1\rangle$  and  $|2\rangle$  become increasingly favorable for chemical reactions as the dipole-dipole interaction strength is increased, for example by increasing the external electric field  $\vec{E}$ . In contrast, channel  $|3\rangle$  has a centrifugal barrier whose height increases for higher dipole moment, within the  $|\vec{E}|$  range considered in this work. This barrier hence continues to

prevent molecules from reaching short range.

Fig. 1 C shows how these different collision channels can be accessed through control of the internal molecular states and the  $\hat{z}$  motional states. In Fig. 1 C, molecules in different internal states are shown in different colors and the harmonic oscillator states in  $\hat{z}$  are labeled by  $v$ . In case (1), for two molecules in different internal molecular states and in any combination of  $v$  levels, channel  $|1\rangle$  is allowed when  $\eta = -1$ , resulting in no centrifugal barrier. In case (2), when the molecules are prepared in identical internal molecular states but in different  $v$  levels, the lowest energy collision channel is  $|2\rangle$  (“head-to-tail”), which is allowed when  $\gamma = -1$ . In case (3), where the molecules are prepared in the same internal state and the same  $v$  level, the two lower energy collision channels are no longer allowed, and reactions can only proceed through channel  $|3\rangle$  (“side-by-side”). This case is the least favorable for atom-exchange bimolecular chemical reactions.

We create a trapped, ultracold gas of  $^{40}\text{K}^{87}\text{Rb}$  molecules, in their lowest energy ro-vibrational level and in a single hyperfine state [20], following the techniques described in Ref. [21]. To confine the molecules, we start with a crossed-beam optical dipole trap, with a harmonic trapping frequency of 180 Hz along the vertical direction ( $\hat{z}$ ) and 25 Hz in the transverse directions. For the current work, we add an optical lattice along  $\hat{z}$ , which is formed by a retro-reflected beam with a  $1/e^2$  waist of 250  $\mu\text{m}$  and a wavelength of 1064 nm. Both optical dipole trap beams and the optical lattice beam are linearly polarized and their polarizations are mutually orthogonal. Each layer of the optical lattice trap is tightly confining in  $\hat{z}$  with a harmonic trapping frequency of  $\nu_z = 23$  kHz for the molecules, while in the transverse directions, the combined trap has a harmonic trapping frequency of 36 Hz. The tunneling rate between lattice layers is negligible and, therefore, each layer realizes an isolated trap for the molecules. Initially, 34,000 ground-state molecules are confined in

roughly 23 layers, with the center layer having 2200 molecules and a peak density of  $3.4 \times 10^7 \text{ cm}^{-2}$ .

We start by loading ultracold  $^{40}\text{K}$  and  $^{87}\text{Rb}$  atoms from the crossed-beam dipole trap into the combined trap by turning up the intensity of the optical lattice beam in 150 ms. We then create molecules in the lattice by first forming extremely weakly bound molecules through magneto-association of atom pairs and then coherently transferring these molecules into their ro-vibrational ground state using optical transitions [21]. The temperature of the molecular gas,  $T$ , in the combined optical dipole plus lattice trap can be varied between 500 nK and 800 nK by varying the initial atom gas conditions. To completely freeze out motion of the molecules along  $\hat{z}$  requires that  $k_B T \ll h\nu_z$ , where  $k_B$  is Boltzmann's constant. For a gas at  $T = 800$  nK in our lattice,  $\frac{k_B T}{h\nu_z} = 0.72$ , and we expect 25% of the molecules will occupy higher  $v$  levels.

As discussed above, in order to control the stereochemistry of bimolecular reactions in the ultracold gas, we need to control both the internal state and the harmonic oscillator level  $v$  of the molecules. We create the molecules in a single internal quantum state. If desired, we can subsequently create a 50/50 mixture of molecules in the ground and first excited rotational states by applying a resonant microwave  $\pi/2$ -pulse [20]. The occupation of lattice levels  $v$  can be controlled by varying  $T$ ; alternatively, we can prepare a non-thermal distribution of molecules using parametric heating. Here, the lattice intensity is modulated at twice  $\nu_z$ , and, as a result, molecules initially in the  $v = 0$  level are excited to the  $v = 2$  level.

We determine the population in each lattice level using an adiabatic band-mapping technique [22, 23]. As the lattice potential is ramped down slowly, molecules in different vibrational levels of the lattice are mapped onto Brillouin zones. The measured molecule

momentum distribution following this ramp is shown in Fig. 2 A for a  $T = 800$  nK molecular gas. The measured fraction in  $v = 0$  matches well with the expected thermal distribution. In contrast, Fig. 2 B shows the measured non-equilibrium occupation of lattice vibrational levels following parametric heating.

We measure the bimolecular reaction rate by monitoring the loss of trapped molecules as a function of time. To image the molecules, we reverse our coherent transfer process to bring the molecules back to a weakly bound state where we can detect the molecules with time-of-flight absorption imaging [21]. The molecules are imaged after free expansion from the combined optical dipole plus lattice trap. From the images, we obtain the total number of molecules and the radial cloud size. Since we do not resolve the individual layers of the optical lattice, we obtain an average 2D density per layer by dividing the total number by the cross-sectional area of the cloud, and by an effective number of layers  $\alpha$ , as defined in the Methods section.

In Fig. 3 A, we show the average 2D density as a function of time. For these data, the molecules are all prepared in the same internal state and  $|\vec{E}|$  is 4 kV/cm, which gives an induced molecular dipole moment of 0.158 Debye (D), where  $1\text{D} = 3.336 \times 10^{-30}$  C·m. The two data sets in Fig. 3 A correspond to an unperturbed  $T = 800$  nK gas (black squares) and a parametrically heated gas (red circles). For the case where parametric heating was used to increase population in  $v > 0$  levels, the data show a faster initial loss of molecules. This suggests that the initial loss is predominately due to interlevel collisions as described in case (2) of Fig. 1 C, while intralevel collisions (case (3) of Fig. 1 C) give a slower loss of molecules at longer times.

We fit the data using a simple model, which assumes two loss rate constants: one for interlevel collisions,  $\beta_{|2)}$ , and a second one for intralevel collisions,  $\beta_{|3)}$  (with the subscripts



referring to the adiabatic channels labeled in Fig. 1 B). Here,

$$\begin{aligned}
\frac{dn_0}{dt} &= -\beta_{|3\rangle}n_0^2 - \beta_{|2\rangle}n_0n_1 - \beta_{|2\rangle}n_0n_2, \\
\frac{dn_1}{dt} &= -\beta_{|2\rangle}n_0n_1 - \beta_{|3\rangle}n_1^2 - \beta_{|2\rangle}n_1n_2, \\
\frac{dn_2}{dt} &= -\beta_{|2\rangle}n_0n_2 - \beta_{|2\rangle}n_1n_2 - \beta_{|3\rangle}n_2^2,
\end{aligned}
\tag{3}$$

where  $n_v$  is the 2D density of molecules in a particular lattice vibrational level  $v$ . To fit the measured time dependence of the total 2D density,  $n_{\text{tot}}(t)$ , we use  $n_{\text{tot}}(t) = n_0(t) + n_1(t) + n_2(t)$ . We input the measured initial populations  $n_v/n_{\text{tot}}$  (see Fig. 2 and Methods) at  $t = 0$ , and we fit the data to the numerical solution of Eqn. 3. We obtain  $\beta_{|3\rangle}$  and  $\beta_{|2\rangle}$  from a simultaneous fit to the two measured  $n_{\text{tot}}(t)$  curves shown in Fig. 3 A.

By repeating this procedure for different values of  $|\vec{E}|$ , we measure the chemical reaction rate constants,  $\beta_{|3\rangle}$  and  $\beta_{|2\rangle}$ , as a function of the induced dipole moment. In Fig. 3 B, we show the intralevel (black squares) and interlevel (red circles) chemical rate constants as a function of the dipole moment. Also shown as green triangles in Fig. 3 B are the results of two measurements for a 50/50 mixture of molecules in different rotational states (case (1) of Fig. 1 C). Here, we fit the loss of molecules in the ground rotational state to the solution of  $\frac{dn_{\text{tot}}}{dt} = -\beta_{|1\rangle}n_{\text{tot}}^2$  to extract a single loss rate constant.

For comparison with these measurements, we perform quantum scattering calculations using a time-independent quantum formalism based on spherical coordinates with cylindrical asymptotic matching to describe the molecular collisions in quasi-2D [24]. We use an absorbing potential at short distance to represent chemical reactions [18, 25]. This technique showed excellent agreement with previous experimental data for KRb bimolecular reactions in 3D [4, 5]. We computed the loss rate coefficients  $\beta_{v_1, v_2}$  for molecules in different initial lattice vibrational states  $v_1, v_2$ , at a collision energy of 800 nK. When the induced dipole

moment is still small ( $0 - 0.2 D$ ), the measured temperature is a good approximation for the mean collision energy. The loss rates of the different processes can be separated into fast loss rates ( $\beta_{0,1}, \beta_{0,2}, \beta_{1,2} \approx \beta_{|2\rangle}$ ) and slow loss rates ( $\beta_{0,0}, \beta_{1,1}, \beta_{2,2} \approx \beta_{|3\rangle}$ ). The black theoretical curve in Fig. 3 B corresponds to an average of the slow rates weighted by the initial populations  $n_0, n_1, n_2$ . The red curve corresponds to the same average but for the fast rates. The green curve corresponds to the loss rate of molecules in different internal states.

The three measured reaction rate constants shown in Fig. 3 B are consistent with the quantum scattering calculations for the collision channels shown in matching colors in Fig. 1 B and Fig. 1 C. Molecules in different rotational states (green triangles in Fig. 3 B) have the highest rate for chemical reactions, consistent with the fact that they can collide in channel  $|1\rangle$ , which corresponds to spatially isotropic collisions with no centrifugal barrier. On the other hand, molecules prepared in the same internal molecular state (red circles and black squares in Fig. 3 B) have suppressed reaction rates because the lowest energy collision channel is no longer allowed. Instead, identical molecules in different lattice levels (red circles in Fig. 3 B) react predominantly through collisions in channel  $|2\rangle$ , or “head-to-tail”, while identical molecules in the same lattice level (black squares in Fig. 3 B) react through collisions in channel  $|3\rangle$ , or “side-by-side”. The importance of stereodynamics on the reaction rate for polar molecules is manifest in the very different dipole-moment dependence of the reactions rates in these two collision channels. In particular, for the case where the molecules are prepared both in the same internal quantum state and in the same  $v$  level, the reaction rate is suppressed even as the dipole moment is increased.

Figure 4 shows how the initial loss rate in a gas of identical molecules depends on the fractional occupation of the lowest lattice level,  $n_0/n_{\text{tot}}$ . As  $n_0/n_{\text{tot}}$  increases, the calculated initial loss rate constant for a molecular gas in thermal equilibrium (solid black line) changes

from close to  $\beta_{|2\rangle}$  (the red line indicating the measured value at 0.174 D from Fig. 3 B) to  $\beta_{|3\rangle}$  (open point at  $n_0/n_{\text{tot}} = 1$ ). In thermal equilibrium, the fractional occupation of the lowest vibrational level is given by the Boltzmann distribution (see Methods). On the top axis of Fig. 4, we give the corresponding values of the scaled temperature  $\frac{k_B T}{h\nu_z}$ . The solid triangles in Fig. 4 correspond to the measured initial loss rate at different temperatures (500 nK and 800 nK), while the open symbol at  $n_0/n_{\text{tot}} \approx 0.5$  corresponds to the initial loss rate for the parametrically heated, non-thermal molecular gas.

We also directly compare the suppressed chemical reaction rate in quasi-2D to that of the 3D case in the inset to Fig. 4. Here, we compare data for a 3D geometry from Ref. [5] against the suppressed loss rate constant measured in quasi-2D. For the comparison, the 2D loss rate is scaled to 3D using  $\beta_{3D} = \sqrt{\pi} a_{ho} \beta_{2D}$  [19, 27, 28], where  $a_{ho}$  is the harmonic oscillator length in  $\hat{z}$ . For a dipole moment  $d$  greater than 0.1 D, the 3D loss rate constant increases dramatically as  $d^6$  [5, 26], whereas the scaled loss rate constant for the quasi-2D case remains close to the value at zero electric field. At a dipole moment of 0.174 D, the measured suppression in quasi-2D is a factor of 60.

The results shown here demonstrate how quantum stereochemistry in the ultracold regime can be used to control reaction rates. The capability of precisely controlling the molecular quantum states for both the internal and external degrees of freedom is a key ingredient for this advance. The strong suppression of reaction rates for a gas of fermionic molecules in a quasi-2D geometry opens the door for creating a stable ultracold gas of polar molecules and studying the many-body physics of such a system. This approach is particularly appealing considering that a number of bialkali polar molecular species currently under study are expected to experience chemical reactions at rates similar to the KRb case [19, 29–31].

## Methods Summary

The traces in Fig. 2 were obtained by averaging the images in the transverse direction within one rms width of the Gaussian distribution. We fit the traces to the convolution of a series of step functions and a Gaussian: the former describes the first three Brillouin zones whereas the latter characterizes the effect of a finite imaging resolution. The uncertainty in the relative population is 3%, and is dominated by systematic errors arising from the variation of the imaging resolution within the range of 1 to 2 pixels.

The average 2D density shown in Fig. 3 A is obtained by dividing the total number of molecules,  $N$ , by an effective area,  $4\pi\alpha\sigma_r^2$ , where  $\sigma_r$  is the rms cloud size in the transverse direction and  $N/\alpha$  is a number-weighted average over the occupied lattice layers. We calculate  $\alpha(t = 0) = 23$  assuming an initial discrete Gaussian distribution in  $\hat{z}$  with an rms width that we measure after transferring the molecules back to the optical dipole trap. However,  $\alpha$  increases at longer times because of the density dependence of the loss. For our analysis, we use a time-averaged value  $\alpha = 30$  that was determined by comparing an analysis based on a uniform layer density to a numerical simulation of the loss in each layer. The uncertainties for  $\beta_{|3\rangle}$  and  $\beta_{|2\rangle}$  are dominated by statistical uncertainties in the fits to  $n_{\text{tot}}(t)$ . For the data shown in green triangles in Fig. 3 B, the two internal molecular states are  $|0, 0, -4, 1/2\rangle$  and  $|1, 1, -4, 1/2\rangle$ , following the notation of Ref. [20].

For the solid black line in Fig. 4, the fractional molecular population  $f(v, T)$  in a vibrational level  $v$  at temperature  $T$  is obtained from a Boltzmann distribution, and the effective  $\beta_{\text{initial}}$  is then calculated as

$$\beta_{\text{initial}} = \beta_{|3\rangle} \sum_v f(v, T)^2 + \beta_{|2\rangle} \sum_{v_1 \neq v_2} f(v_1, T)f(v_2, T). \quad (4)$$

## Acknowledgments

We thank P. Julienne, P. Zoller, G. Pupillo, and A. Micheli for stimulating discussions and S. Moses for technical contributions. We gratefully acknowledge financial support for this work from NIST, NSF, AFOSR-MURI, DOE, and DARPA.

---

- [1] Zare, R. N. Laser control of chemical reactions. *Science* **279**, 1875-1879 (1998).
- [2] Aldegunde, J. *et al.* How reactants polarization can be used to change and unravel chemical reactivity. *J. Phys. Chem. A* **109**, 6200-6217 (2005).
- [3] Gijbbersen, A., Linnartz, H., Taatjes, C. A., Stolte, S. Quantum interference as the source of steric asymmetry and parity propensity rules in NO-rare gas inelastic scattering. *J. Am. Chem. Soc.* **128**, 8777-8789 (2006).
- [4] Ospelkaus, S. *et al.* Quantum-state controlled chemical reactions of ultracold KRb molecules. *Science*, **327**, 853-857 (2010).
- [5] Ni, K.-K. *et al.* Dipolar collisions of polar molecules in the quantum regime. *Nature* **464**, 1324-1328 (2010).
- [6] Büchler, H. P. *et al.* Strongly correlated 2D quantum phases with cold polar molecules: Controlling the shape of the interaction potential. *Phys. Rev. Lett.* **98**, 060404 (2007).
- [7] Micheli, A. *et al.* Cold polar molecules in two-dimensional traps: Tailoring interactions with external fields for novel quantum phases. *Phys. Rev. A* **76**, 043604 (2007).
- [8] Pupillo, G., Micheli, A. Büchler, H. P., Zoller, P. in *Cold Molecules: Theory, Experiment, Applications* (eds. Krems, R. V., Friedrich, B., Stwalley, W. C.) 421-469 (CRC, 2009)
- [9] Baranov, M. Theoretical progress in many-body physics with ultracold dipolar gases. *Phys.*

- Rep.* **464**, 71-111 (2008).
- [10] Lahaye, T., Menotti, C., Santos, L., Lewenstein, M., Pfau, T. The physics of dipolar bosonic quantum gases. *Rep. Prog. Phys.* **72**, 126401 (2009).
- [11] Wang, D. W., Lukin, M. D., Demler, E. Quantum fluids of self-assembled chains of polar molecules. *Phys. Rev. Lett.* **97**, 180413 (2006).
- [12] Klawunn, M., Duhme, J., Santos, L. Bose-Fermi mixtures of self-assembled filaments of fermionic polar molecules. *Phys. Rev. A* **81**, 013604 (2010).
- [13] Capogrosso-Sansone, B. *et al.* Quantum Phases of Cold Polar Molecules in 2D Optical Lattices *Phys. Rev. Lett.* **104**, 125301 (2010).
- [14] Sawyer, B. C., *et al.* Cold heteromolecular dipolar collisions. *arXiv:1008.5127* (2010).
- [15] Krens, R. V. Molecules near absolute zero and external field control of atomic and molecular dynamics. *Int. Rev. Phys. Chem.* **24**, 99-118 (2005).
- [16] Carr, L. D., *et al.* Cold and ultracold molecules: science, technology and applications. *New J. Phys.* **11**, 055049 (2009).
- [17] Ticknor, C. Quasi-two-dimensional dipolar scattering. *Phys. Rev. A* **81**, 042708 (2010).
- [18] Quéméner, G., Bohn, J. L. Electric field suppression of ultracold confined chemical reactions. *Phys. Rev. A* **81**, 060701 (2010).
- [19] Micheli, A. *et al.* Universal rates for reactive ultracold polar molecules in reduced dimensions. *Phys. Rev. Lett.* **105**, 073202 (2010).
- [20] Ospelkaus, S. *et al.* Controlling the hyperfine state of rovibronic ground state polar molecules. *Phys. Rev. Lett.* **104**, 030402 (2010).
- [21] Ni, K.-K. *et al.* A high-phase-space-density gas of polar molecules. *Science* **322**, 231-235 (2008).

- [22] Kastberg, A., Phillips, W. D., Rolston, S. L., Spreew, R. J. C., Jessen, P. S. Adiabatic cooling of cesium to 700 nK in an optical lattice. *Phys. Rev. Lett.* **74**, 1542-1545 (1995).
- [23] Greiner, M., Bloch, I., Mandel, O., Hänsch, T. W., Esslinger, T. Exploring phase coherence in a 2D lattice of Bose-Einstein condensates. *Phys. Rev. Lett.* **87**, 160405 (2001).
- [24] Quéméner, G., Bohn, J. L. Dynamics of molecules in confined geometry and electric field. in preparation (2010).
- [25] Idziaszek, Z., Julienne, P. S. Universal Rate Constants for Reactive Collisions of Ultracold Molecules. *Phys. Rev. Lett.* **104**, 113202 (2010).
- [26] Quéméner, G., Bohn, J. L. Strong dependence of ultracold chemical rates on electric dipole moments. *Phys. Rev. A* **81**, 022702 (2010).
- [27] Petrov, D. S., Shlyapnikov, G. V., Interatomic collisions in a tightly confined Bose gas. *Phys. Rev. A* **64**, 012706 (2001).
- [28] Li, Z., Krems, R. V. Inelastic collisions in an ultracold quasi-two-dimensional gas. *Phys. Rev. A* **79**, 050701(R) (2009).
- [29] Zuchowski, P. S., Hutson, J. M. Reactions of ultracold alkali metal dimers. *Phys. Rev. A* **81**, 060703 (2010).
- [30] Byrd, J. N., Montgomery, J. A. Jr., Côté, R. Structure and thermochemistry of  $K_2Rb$ ,  $KRb_2$ , and  $K_2Rb_2$ . *Phys. Rev. A* **82**, 010502 (2010).
- [31] Meyer, E. R., Bohn, J. L. Product-state control of bi-alkali-metal chemical reactions. *arXiv:1004.3317* (2010).

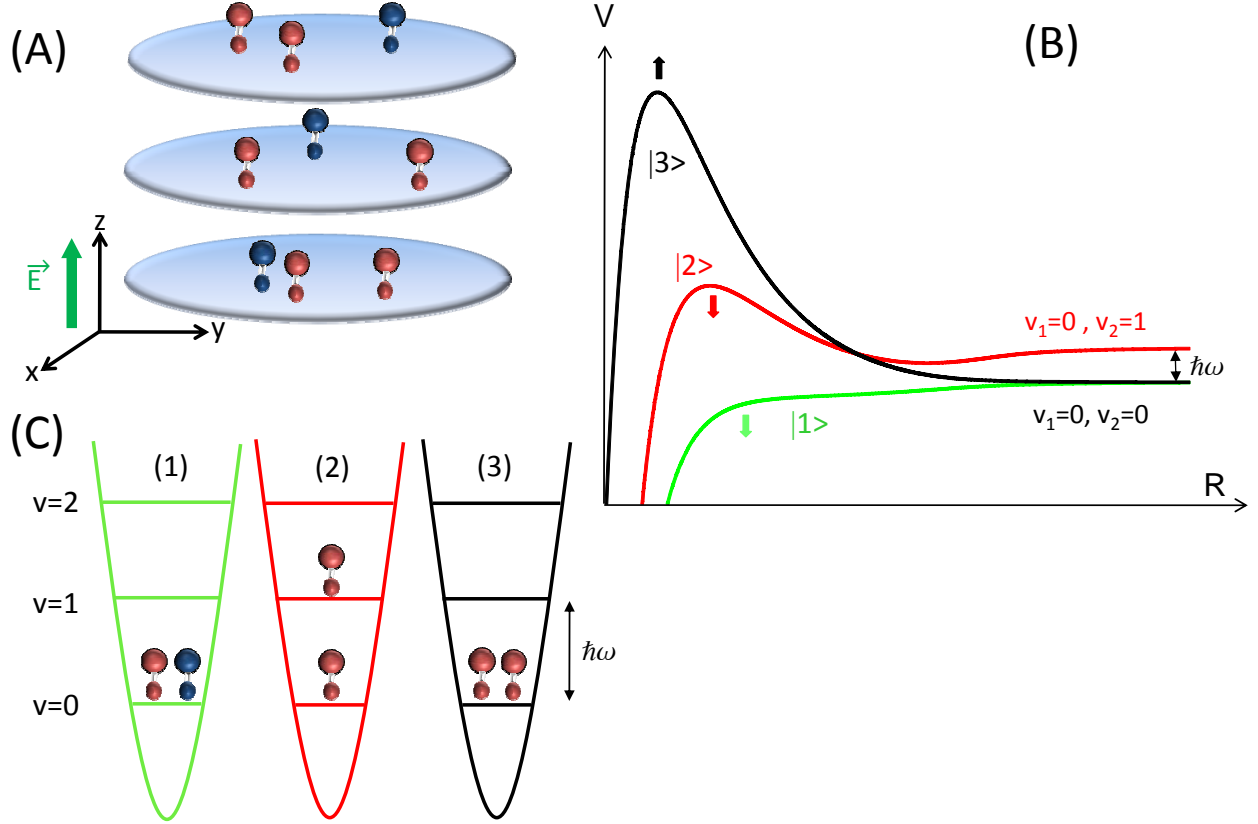


FIG. 1: **Quantized stereodynamics of ultracold chemical reactions in quasi-2D.** (A) A quasi-2D geometry for collisions is realized for polar molecules confined in a one-dimensional optical lattice. An external electric field is applied along the tight confinement axis. (B) The lowest three adiabatic potentials for collisions are shown schematically as a function of the intermolecular separation,  $R$ . These three channels are ordered with increasing magnitude of the centrifugal barrier. The arrows indicate the change in the potential for an increasing external electric field, and hence a growing induced dipole moment. (C) Three different cases are shown schematically for each of the three lowest collision channels. The lowest energy collision channel occurs when two molecules are prepared in different internal states (indicated here by the colors of the molecules). The second channel is realized when two identical molecules are prepared in different vibrational levels  $v$  for their  $\hat{z}$  motions. The third case has a much reduced loss rate as a consequence of an increased centrifugal barrier when the two identical molecules are prepared in the same vibrational level along  $\hat{z}$ .



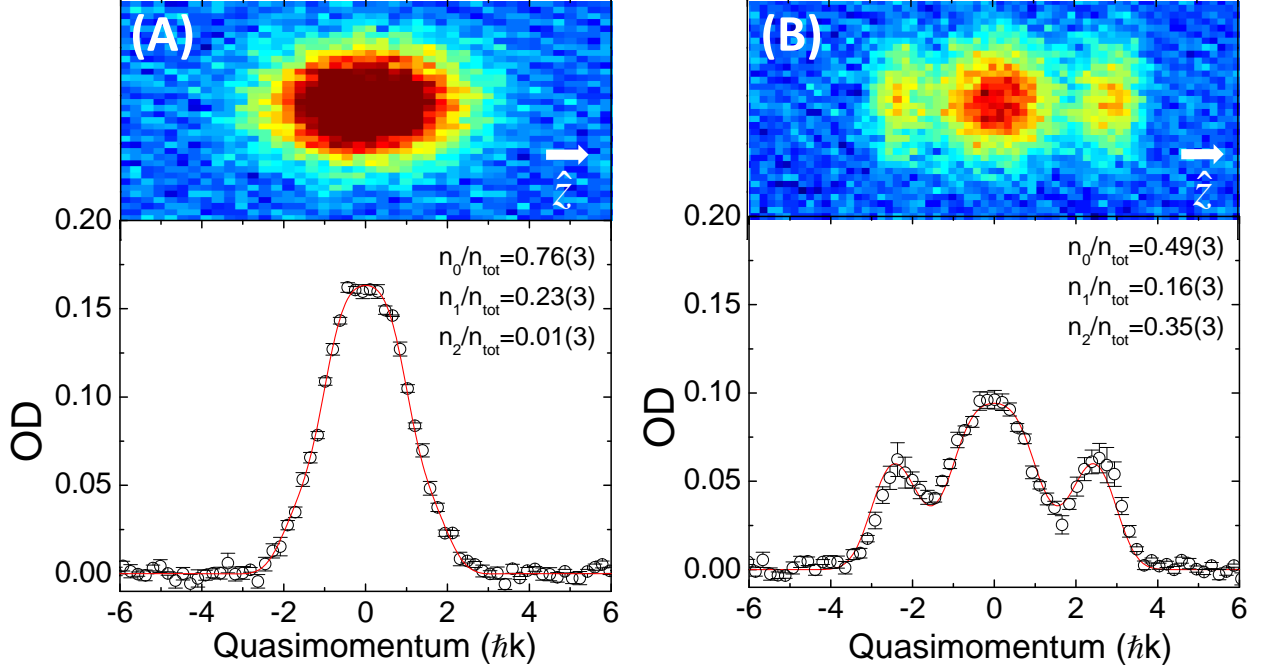


FIG. 2: **Relative population of molecules in the lattice vibrational levels.** We measure the relative population in each lattice vibrational level using a band-mapping technique. The results are shown for (A) a thermal distribution of molecules and (B) a non-thermal distribution created by parametric heating in  $\hat{z}$ . The two images use the same color scale for the optical depth (OD). The images are an average of 5 shots and 7 shots for (A) and (B), respectively, taken after 10 ms of free expansion. Below each image we show a trace along  $\hat{z}$  that corresponds the OD averaged over the transverse direction. A fit (red line) to the trace, which takes into account both the size of the Brillouin zones and our imaging resolution, is used to extract the relative populations,  $n_v/n_{\text{tot}}$ , in each lattice level  $v$ . The horizontal axis corresponds to momentum in  $\hat{z}$  and is marked in units of the lattice momentum  $\hbar k$ , where  $k$  is the lattice wavevector.

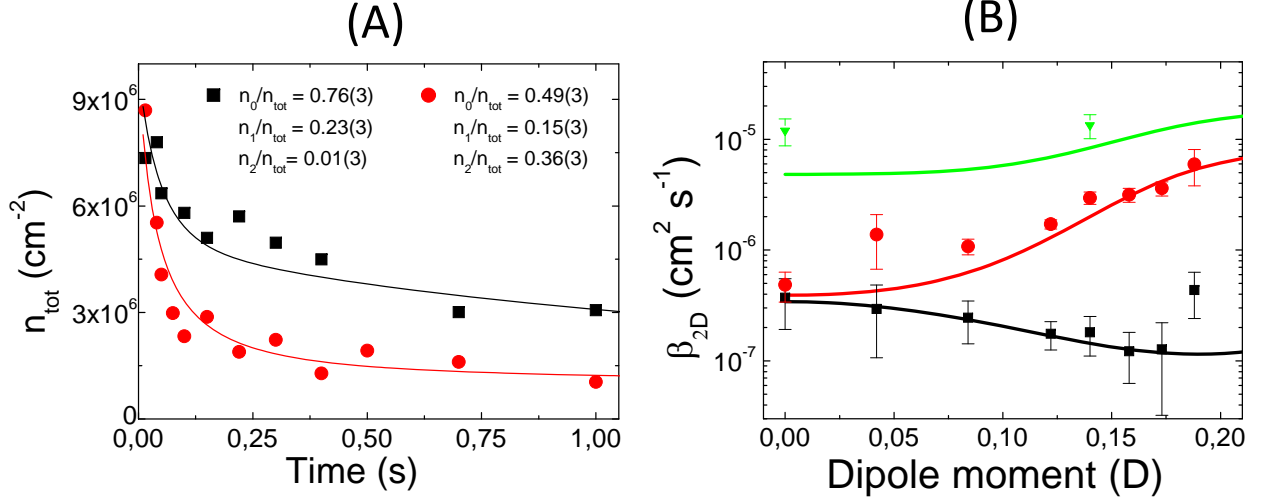


FIG. 3: **Measurements of 2D loss rates and comparison with theory.** (A) A fit (solid lines) to the measured loss curves, with (red circles) and without (black squares) 0.3 ms of parametric heating in  $\hat{z}$ , is used to extract the loss rate constants  $\beta_{|3\rangle}$  and  $\beta_{|2\rangle}$ . (B) The extracted loss rate constants for collisions of molecules in the same lattice vibrational level (black squares) and from different lattice vibrational levels (red circles) are plotted for several dipole moments. Measured loss rate constants for molecules prepared in different internal states are shown as green triangles. For comparison with each of these three measurements, we include a quantum scattering calculation for  $\nu_z = 23$  kHz,  $T = 800$  nK (solid lines). The potentials corresponding to the dominant loss channel for the three cases are shown in matching colors in Fig. 1 B.

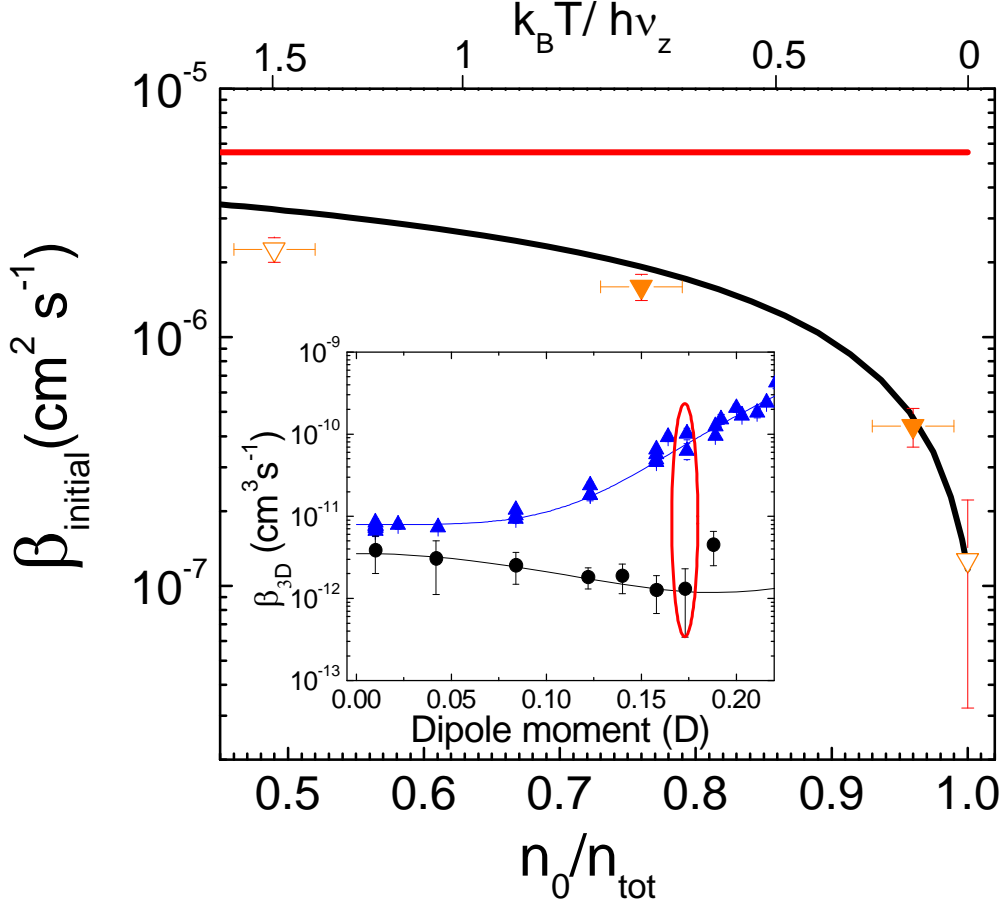


FIG. 4: **Loss rates from 3D to 2D.** The effective initial loss rate,  $\beta_{\text{initial}}$ , for polar molecules confined in a 2D geometry depends on the fractional population ( $n_0/n_{\text{tot}}$ ) in the lowest harmonic oscillator level in  $\hat{z}$ , which for a gas in thermal equilibrium depends on the ratio  $\frac{k_B T}{h\nu_z}$ . The measured initial loss rates for a dipole moment of 0.174 D are displayed for two different thermal distributions (solid triangles), a non-thermal sample created by parametric heating (the top open triangle), and an extracted pure  $\beta_{|3\rangle}$  when the entire population is residing in the lattice ground vibrational level (the bottom open triangle). The experimental results agree well with a simple model (black curve) described in the text and Methods. The top line indicates the value of  $\beta_{|2\rangle}$  as measured in Fig. 3 B. (Inset) The intralevel loss rate for identical fermionic KRb molecules in 2D (black circles) is compared with the loss rate in 3D (blue triangles). The 3D data for  $T = 300$  nK are borrowed from Ref. [5]. The 2D data were taken at  $T = 800$  nK and are converted to 3D rates by multiplication with  $\sqrt{\pi}a_{ho}$ , where  $a_{ho}$  is the harmonic oscillator length in  $\hat{z}$ .